Renewable and Sustainable Energy Reviews 36 (2014) 236–246

Contents lists available at ScienceDirect

Renewable and Sustainable Energy Reviews

journal homepage: www.elsevier.com/locate/rser

An overview of distributed activation energy model and its application in the pyrolysis of lignocellulosic biomass

Junmeng Cai [a,b,*], Weixuan Wu [a], Ronghou Liu [a]

[a] Biomass Energy Engineering Center, Key Laboratory of Urban Agriculture (South) Ministry of Agriculture, School of Agriculture and Biology, Shanghai Jiao Tong University, 800 Dongchuan Road, Shanghai 200240, PR China
[b] State Key Laboratory of Heavy Oil Processing, China University of Petroleum, 18 Fuxue Road, Beijing 102249, PR China

ARTICLE INFO

Article history:
Received 5 August 2013
Received in revised form
27 February 2014
Accepted 27 April 2014
Available online 20 May 2014

Keywords:
Distributed activation energy model (DAEM)
Lignocellulosic biomass
Pyrolysis
Kinetics
Parameter estimation method
Numerical calculation

ABSTRACT

Research interest in the conversion of lignocellulosic biomass into energy and fuels through the pyrolysis process has increased significantly in the last decade as the necessity for a renewable source of carbon has become more evident. For optimal design of pyrolysis reactors, an understanding of the pyrolysis kinetics of lignocellulosic biomass is of fundamental importance. The distributed activation energy model (DAEM) has been usually used to describe the pyrolysis kinetics of lignocellulosic biomass. In this review, we start with the derivation of the DAEM. After an overview of the activation energy distribution and frequency factor in the DAEM, we focus on the numerical calculation and parameter estimation methods of the DAEM. Finally, this review summarizes recent results published in the literature for the application of the DAEM to the pyrolysis kinetics of lignocellulosic biomass.

Contents

1. Introduction

The pyrolysis of lignocellulosic biomass has attracted considerable attention because it is the thermochemical process that converts lignocellulosic biomass into liquid fuel (bio-oil), which is easy to store and transport when compared to raw biomass [1,2]. Knowledge of the kinetics is important in the computational fluid dynamics modeling of biomass pyrolysis process [3]. And in the pyrolysis process of lignocellulosic biomass, the relative rates of decomposition, cracking, and repolymerization/condensation reactions influence the quantity and quality of bio-oil produced as well as the long-term storage stability of the bio-oil [4].

The distributed activation energy model (DAEM) is a multiple reaction model, which is widely used in the pyrolysis of

* Corresponding author at: Biomass Energy Engineering Center, Key Laboratory of Urban Agriculture (South) Ministry of Agriculture, School of Agriculture and Biology, Shanghai Jiao Tong University, 800 Dongchuan Road, Shanghai 200240, PR China. Tel./fax: +86 21 34206624.
E-mail address: jmcai@sjtu.edu.cn (J. Cai).

http://dx.doi.org/10.1016/j.rser.2014.04.052
1364-0321/

lignocellulosic biomass [5]. The model assumes the decomposition mechanism take a large number of independent, parallel, first-order or nth-order reactions with different activation energies reflecting variations in the bond strengths of species. The difference in activation energies can be represented by a continuous distribution function [6]. The DAEM is not only used to describe the pyrolysis kinetics of lignocellulosic biomass and its main components, but also to describe the pyrolysis kinetics of coal [7–9] and other thermally degradable materials [10–13].

In order to better understand the DAEM and its application in the pyrolysis of lignocellulosic biomass, an overview of the research and development in the DAEM for the pyrolysis of lignocellulosic biomass is conducted. The derivation of the DAEM was first presented. Then, the activation energy distribution and frequency factor in the DAEM are overviewed and the numerical calculation of the DAEM is discussed. In Section 5, the methods for the estimation of the DAEM kinetic parameters are critically studied. Finally, the up-to-date research efforts in the DAEM for the pyrolysis of lignocellulosic biomass are summarized.

2. Derivation of DAEM

The concept of an activation energy distribution was originally proposed by Vand [14] and later used by Pitt [15] and Anthony [16]. The DAEM for lignocellulosic biomass pyrolysis may be applied to either the total amount of volatiles released, or to the amount of an individual volatile constituent. The description in this work follows the total amount volatiles released. It is assumed that lignocellulosic biomass has many chemical groups which are numbered $i=1,\ldots,s$, and the released mass fraction for the ith group is $V_i(t)$. The contribution of the decomposition of the ith group is assumed to be described by the pseudo-nth-order rate equation

$$\frac{\mathrm{d}(V_i/V_i^*)}{\mathrm{d}t}=k_i\left(\frac{V_i^*-V_i}{V_i^*}\right)^n=A_i\exp\left(-\frac{E_i}{RT}\right)\left(\frac{V_i^*-V_i}{V_i^*}\right)^n \tag{1}$$

where V_i^* is the total released mass fraction for the ith group, n is the reaction order and k_i is the reaction rate constant, A_i is the frequency factor, E_i is the activation energy, R is the universal gas constant, T is the temperature, and t is the time.

Eq. (1) can be written in its integral form

$$\frac{V_i}{V_i^*}=\begin{cases}1-\left[1-(1-n)\int_0^t A_i\exp\left(-\frac{E_i}{RT}\right)\mathrm{d}t\right]^{1/(1-n)} & n\neq 1\\ 1-\exp\left[-\int_0^t A_i\exp\left(-\frac{E_i}{RT}\right)\mathrm{d}t\right] & n=1\end{cases} \tag{2}$$

The complexity of lignocellulosic biomass pyrolysis is such that a continuous distribution $f(E)$ of activation energies is assumed where $\int_E^{E+\Delta E} f(E)\mathrm{d}E$ describes the probability that chemical groups with a sample have an activation energy in this range E to $E+\Delta E$. The mass fraction of potential volatile material with activation energies between E and $E+\mathrm{d}E$, $\mathrm{d}V^*$, at a given time t is $V^*f(E)\mathrm{d}E$.

$$\mathrm{d}V^*=V^*f(E)\mathrm{d}E \tag{3}$$

Then, V_i^* and V_i are replaced by $\mathrm{d}V^*$ and $\mathrm{d}V$, respectively. Then Eq. (2) becomes

$$\mathrm{d}V=\begin{cases}V^*\left\{1-\left[1-(1-n)\int_0^t A\exp\left(-\frac{E}{RT}\right)\mathrm{d}t\right]^{1/(1-n)}\right\}f(E)\mathrm{d}E & n\neq 1\\ V^*\left\{1-\exp\left[-\int_0^t A\exp\left(-\frac{E}{RT}\right)\mathrm{d}t\right]\right\}f(E)\mathrm{d}E & n=1\end{cases} \tag{4}$$

The integration of Eq. (4) leads to

$$\alpha=\frac{V}{V^*}=\begin{cases}1-\int_0^\infty\left[1-(1-n)\int_0^t A\exp\left(-\frac{E}{RT}\right)\mathrm{d}t\right]^{1/(1-n)}f(E)\mathrm{d}E & n\neq 1\\ 1-\int_0^\infty\exp\left[-\int_0^t A\exp\left(-\frac{E}{RT}\right)\mathrm{d}t\right]f(E)\mathrm{d}E & n=1\end{cases} \tag{5}$$

where α is the degree of conversion.

Differentiating Eq. (5) with respect to t, the expression of $\mathrm{d}\alpha/\mathrm{d}t$ is

$$\frac{\mathrm{d}\alpha}{\mathrm{d}t}=\begin{cases}\int_0^\infty A\exp\left(-\frac{E}{RT}\right)\left[1-(1-n)\int_0^t A\exp\left(-\frac{E}{RT}\right)\mathrm{d}t\right]^{n/(1-n)}f(E)\mathrm{d}E & n\neq 1\\ \int_0^\infty A\exp\left[-\frac{E}{RT}-\int_0^t A\exp\left(-\frac{E}{RT}\right)\mathrm{d}t\right]f(E)\mathrm{d}E & n=1\end{cases} \tag{6}$$

Most laboratory experiments involving the pyrolysis of lignocellulosic biomass are performed at temperatures linearly varying with time from a starting temperature, T_0 [17]. Under the linear heating program, Eqs. (5) and (6) can be rewritten as Eqs. (7) and (8)

$$\alpha=\begin{cases}1-\int_0^\infty\left[1-(1-n)\int_{T_0}^T\frac{A}{\beta}\exp\left(-\frac{E}{RT}\right)\mathrm{d}T\right]^{1/(1-n)}f(E)\mathrm{d}E & n\neq 1\\ 1-\int_0^\infty\exp\left[-\int_{T_0}^T\frac{A}{\beta}\exp\left(-\frac{E}{RT}\right)\mathrm{d}T\right]f(E)\mathrm{d}E & n=1\end{cases} \tag{7}$$

$$\frac{\mathrm{d}\alpha}{\mathrm{d}T}=\begin{cases}\int_0^\infty\frac{A}{\beta}\exp\left(-\frac{E}{RT}\right)\left[1-(1-n)\int_{T_0}^T\frac{A}{\beta}\exp\left(-\frac{E}{RT}\right)\mathrm{d}T\right]^{n/(1-n)}f(E)\mathrm{d}E & n\neq 1\\ \int_0^\infty\frac{A}{\beta}\exp\left[-\frac{E}{RT}-\int_{T_0}^T\frac{A}{\beta}\exp\left(-\frac{E}{RT}\right)\mathrm{d}T\right]f(E)\mathrm{d}E & n=1\end{cases} \tag{8}$$

where β is the heating rate.

3. $f(E)$ and A in DAEM

A popular choice for the activation energy distribution is the Gaussian distribution centered at E_0 with standard deviation σ

$$f(E)=\frac{1}{\sigma\sqrt{2\pi}}\exp\left[-\frac{(E-E_0)^2}{2\sigma^2}\right] \tag{9}$$

The disadvantage of the Gaussian distribution is that it is symmetric whereas the actual reactivity distributions tend to be asymmetric [18]. The asymmetry can be accounted for by replacing the Gaussian distribution with other distributions, e.g. the Weibull [19–21] or Logistic [22,23] distributions.

The Weibull distribution was first proposed to describe chemical reactivity distributions for the pyrolysis of petroleum source rocks [19]. For the Weibull distribution, $f(E)$ is given by

$$f(E)=\frac{\lambda}{\eta}\left(\frac{E-\gamma}{\eta}\right)^{\lambda-1}\exp\left[-\left(\frac{E-\gamma}{\eta}\right)^{\lambda}\right] \tag{10}$$

where λ is the shape parameter, η is the width parameter, and γ is the activation energy threshold ($E\geq\gamma$). The mean activation energy E_0 and the standard deviation σ of the Weibull distribution are defined by

$$E_0=\gamma+\eta\Gamma\left(1+\frac{1}{\lambda}\right) \tag{11}$$

$$\sigma=\sqrt{\eta^2\Gamma^2\left(\frac{2}{\lambda}+1\right)-\eta^2\Gamma^2\left(\frac{1}{\lambda}+1\right)} \tag{12}$$

where Γ is the Gamma function. Because of the activation energy threshold, Eqs. (7) and (8) should be written in the following forms if the Weibull distribution is considered

$$\alpha = \begin{cases} 1 - \int_{\gamma}^{\infty} \left[1-(1-n)\int_{T_0}^{T} \frac{A}{\beta}\exp\left(-\frac{E}{RT}\right)\mathrm{d}T\right]^{1/(1-n)} \frac{\lambda}{\eta}\left(\frac{E-\gamma}{\eta}\right)^{\lambda-1} \exp\left[-\left(\frac{E-\gamma}{\eta}\right)^{\lambda}\right]\mathrm{d}E & n \neq 1 \\ 1 - \int_{\gamma}^{\infty} \exp\left[-\int_{T_0}^{T} \frac{A}{\beta}\exp\left(-\frac{E}{RT}\right)\mathrm{d}T\right] \frac{\lambda}{\eta}\left(\frac{E-\gamma}{\eta}\right)^{\lambda-1} \exp\left[-\left(\frac{E-\gamma}{\eta}\right)^{\lambda}\right]\mathrm{d}E & n = 1 \end{cases} \tag{13}$$

$$\frac{\mathrm{d}\alpha}{\mathrm{d}T} = \begin{cases} \int_{\gamma}^{\infty} \frac{A}{\beta}\exp\left(-\frac{E}{RT}\right)\left[1-(1-n)\int_{T_0}^{T} \frac{A}{\beta}\exp\left(-\frac{E}{RT}\right)\mathrm{d}T\right]^{n/(1-n)} \frac{\lambda}{\eta}\left(\frac{E-\gamma}{\eta}\right)^{\lambda-1} \exp\left[-\left(\frac{E-\gamma}{\eta}\right)^{\lambda}\right]\mathrm{d}E & n \neq 1 \\ \int_{\gamma}^{\infty} \frac{A}{\beta}\exp\left[-\frac{E}{RT} - \int_{T_0}^{T} \frac{A}{\beta}\exp\left(-\frac{E}{RT}\right)\mathrm{d}T\right] \frac{\lambda}{\eta}\left(\frac{E-\gamma}{\eta}\right)^{\lambda-1} \exp\left[-\left(\frac{E-\gamma}{\eta}\right)^{\lambda}\right]\mathrm{d}E & n = 1 \end{cases} \tag{14}$$

The Logistic distribution was presented in our previous paper [22] and was successfully applied to describe the pyrolysis kinetics of cellulose [23] and grape residues [24]. For the Logistic distribution, $f(E)$ is given by

$$f(E) = \frac{\pi}{\sqrt{3}\sigma} \frac{\exp\left[-(\pi(E-\mu)/\sqrt{3}\sigma)\right]}{\{1+\exp\left[-(\pi(E-\mu)/\sqrt{3}\sigma)\right]\}^2} \tag{15}$$

where μ and σ are the mean value and standard deviation of the Logistic distribution.

Capralis et al. studied the pyrolysis of two coals and found that the coal pyrolysis process can be divided into two steps: the tar and light hydrocarbon gas formation during the primary pyrolysis and the char condensation, cross-linking reactions, and a further gas production during the secondary pyrolysis [9]. To better describe the kinetic behavior, the authors proposed a double-Gaussian distribution to present the reactivity distribution [9]

$$f(E) = wf_1(E) + (1-w)f_2(E) \tag{16}$$

where $f_1(E)$ and $f_2(E)$ are Gaussian distributions, and w is the weight parameter.

There are three ways to deal with the frequency factor in the literature. The conventional method to use the DAEM is to select a constant frequency factor value for all reactions (i.e. $1.67 \times 10^{13}\ \mathrm{s}^{-1}$ for coal pyrolysis [8], and $10^{14.13}$, $10^{13.71}$ and $10^{13.90}\ \mathrm{s}^{-1}$ for the pyrolysis of hemicellulose, cellulose, and lignin, respectively [25]). If A is a constant, Eqs. (7) and (8) can be rewritten into the following equations

$$\alpha = \begin{cases} 1 - \int_{0}^{\infty} \left[1-(1-n)\frac{A}{\beta}\int_{T_0}^{T} \exp\left(-\frac{E}{RT}\right)\mathrm{d}T\right]^{1/(1-n)} f(E)\mathrm{d}E & n \neq 1 \\ 1 - \int_{0}^{\infty} \exp\left[-\frac{A}{\beta}\int_{T_0}^{T} \exp\left(-\frac{E}{RT}\right)\mathrm{d}T\right] f(E)\mathrm{d}E & n = 1 \end{cases} \tag{17}$$

$$\frac{\mathrm{d}\alpha}{\mathrm{d}T} = \begin{cases} \int_{0}^{\infty} \frac{A}{\beta}\exp\left(-\frac{E}{RT}\right)\left[1-(1-n)\frac{A}{\beta}\int_{T_0}^{T} \exp\left(-\frac{E}{RT}\right)\mathrm{d}T\right]^{n/(1-n)} f(E)\mathrm{d}E & n \neq 1 \\ \int_{0}^{\infty} \frac{A}{\beta}\exp\left[-\frac{E}{RT} - \frac{A}{\beta}\int_{T_0}^{T} \exp\left(-\frac{E}{RT}\right)\mathrm{d}T\right] f(E)\mathrm{d}E & n = 1 \end{cases} \tag{18}$$

In the two above equations, the inner $\mathrm{d}T$ integral is

$$\int_{T_0}^{T} \exp\left(-\frac{E}{RT}\right)\mathrm{d}T = I(E,T) - I(E,T_0) \tag{19}$$

where $I(E,T) = \int_0^T \exp\left(-(E/RT)\right)\mathrm{d}T$ is the temperature integral [26,27].

Second, the frequency factor in the DAEM is assumed to be connected with the temperature

$$A = A_0 T^m \tag{20}$$

where A_0 is a constant and the exponent m ranges from -1.5 to 2.5. This dependence of the frequency factor on the temperature in the DAEM was found to be used to describe the pyrolysis kinetics of lignin [28], peanut shell, pistachito shell, and sunflower shell [29].

In this case, Eqs. (17) and (18) become

$$\alpha = \begin{cases} 1 - \int_{0}^{\infty} \left[1-(1-n)\frac{A_0}{\beta}\int_{T_0}^{T} T^m \exp\left(-\frac{E}{RT}\right)\mathrm{d}T\right]^{1/(1-n)} f(E)\mathrm{d}E & n \neq 1 \\ 1 - \int_{0}^{\infty} \exp\left[-\frac{A_0}{\beta}\int_{T_0}^{T} T^m \exp\left(-\frac{E}{RT}\right)\mathrm{d}T\right] f(E)\mathrm{d}E & n = 1 \end{cases} \tag{21}$$

$$\frac{\mathrm{d}\alpha}{\mathrm{d}T} = \begin{cases} \int_{0}^{\infty} \frac{A_0 T^m}{\beta}\exp\left(-\frac{E}{RT}\right)\left[1-(1-n)\frac{A_0}{\beta}\int_{T_0}^{T} T^m \exp\left(-\frac{E}{RT}\right)\mathrm{d}T\right]^{n/(1-n)} f(E)\mathrm{d}E & n \neq 1 \\ \int_{0}^{\infty} \frac{A_0 T^m}{\beta}\exp\left[-\frac{E}{RT} - \frac{A_0}{\beta}\int_{T_0}^{T} T^m \exp\left(-\frac{E}{RT}\right)\mathrm{d}T\right] f(E)\mathrm{d}E & n = 1 \end{cases} \tag{22}$$

In Eqs. (21) and (22), the inner $\mathrm{d}T$ integral becomes

$$\int_{T_0}^{T} T^m \exp\left(-\frac{E}{RT}\right)\mathrm{d}T = I_m(E,T) - I_m(E,T_0) \tag{23}$$

where $I_m(E,T) = \int_0^T T^m \exp\left(-(E/RT)\right)\mathrm{d}T$ is the general temperature integral [30]. Here we especially mention the temperature integral or the general temperature integral in order to better state the numerical solution of the DAEM in the next section.

Finally, the frequency factor in the DAEM is assumed to follow the compensation effect (the effect of an increase of E_0 is partially or completely offset by a 'compensatory' increase in A [31]). The relationship between E_0 and A is most usually represented [25,29,32]

$$\ln A = a + bE_0 \tag{24}$$

where E_0 is the mean value of activation energy distribution, a and b are constants. The value of a is usually close to zero [33].

4. Numerical calculation of DAEM

Due to the fact that there is an inner $\mathrm{d}T$ integral and outer $\mathrm{d}E$ integral in the DAEM, it is very difficult to obtain the exact analytical solution of the DAEM. In the literature, many mathematical approximate approaches were pursued to deal with the DAEM. Suuberg expressed the temperature integral over E in terms of complementary error function [34]. Du et al. used the step function approximation technique to determine the activation energy distribution [35]. Donskoi and McElwain used high order Gauss–Hermite integration to evaluate the outer $\mathrm{d}E$ integral [36]. Rostami et al. presented how it is possible to obtain an approximate closed form of the model by assuming that as conversion proceeds, the functional groups with the lowest activation energies are lost first [37].

Since it is difficult to analytically solve the DAEM, several researchers dealt with the DAEM by means of numerical techniques. Braun and Burnham replaced the upper and lower limits of the outer integral with $E_0+3\sigma$ and $E_0-3\sigma$ and divided the activation energy space into 96 equal intervals [38]. Güneş and Güneş used $500\ \mathrm{kJ\,mol}^{-1}$ as the upper limit of the outer $\mathrm{d}E$ integral and 50 integral intervals [39].

For purposes of numerical calculation of the DAEM, either general purposed mathematical software or a computer program developed in any programming language is used. In this work, we developed a program written in the Mathematica software system to numerically solve the DAEM.

Either the temperature integral or the general temperature integral has no exact analytical solution [40], but they can be numerically solved. In the Mathematica software system, the temperature integral and general temperature integral can be expressed in the following forms

$$I(E,T) = \frac{E}{R}\,\mathrm{Gamma}\left[-1, \frac{E}{RT}\right] \tag{25}$$

$$I_m(E,T) = \left(\frac{E}{R}\right)^{m+1} \mathrm{Gamma}\left[-1-m, \frac{E}{RT}\right] \tag{26}$$

For the outer dE integral, we use the 'NIntegrate' function of the Mathematica software system with the integral limits 0 and $E_0+30\sigma$.

To illustrate the proceeding method, the following theoretically simulated DAEM processes with Gaussian distribution are considered. The kinetic parameter values of the first process are as follows: $A=1.67\times10^{13}$ s^{-1}, $E_0=228$ kJ mol^{-1}, $\beta=10$ K min^{-1}, $n=1$ and $\sigma=0.5\%E_0$, 2.5% E_0, 5.0% E_0, 7.5% E_0 and 10.0% E_0. The values of A, E_0 and β were taken from the literature [8], which were used to describe the pyrolysis kinetics of coal. The parameter values in the second process are identical to the first example except for $\sigma=5.0\%$ E_0 and $n=1.0$, 1.5, 2.0, 2.5, and 3.0 (those n values were used to describe the pyrolysis kinetics of biomass in the literature [41]). Figs. 1 and 2 show the $\alpha-T$ and dα/d$T-T$ curves for the first and second processes. From Figs. 1 and 2, it can be seen that increasing the values of σ makes the reaction profile broader and more symmetric and that increasing the reaction order makes the reaction profile broader and makes it more skewed to high temperature.

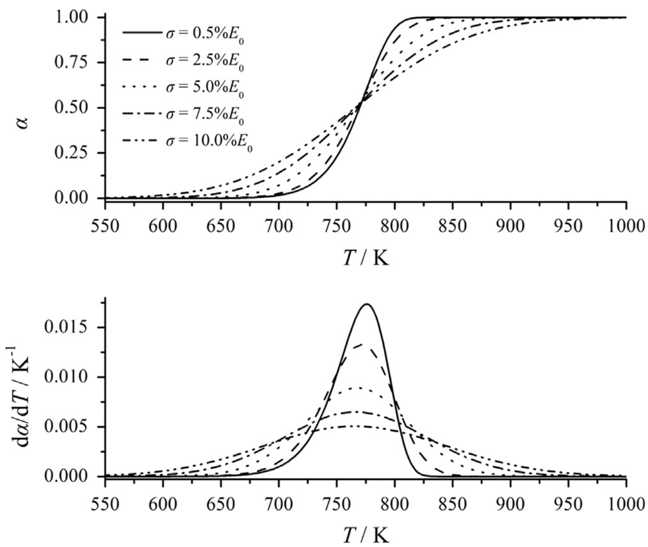

Fig. 1. The simulated $\alpha-T$ and dα/d$T-T$ curves of the Gaussian DAEM processes with the following parameters: $A=1.67\times10^{13}$ s^{-1}, $E_0=228$ kJ mol^{-1}, $\beta=10$ K min^{-1}, $n=1.0$, and $\sigma=0.5\%$ E_0, 2.5% E_0, 5.0% E_0, 7.5% E_0 and 10.0% E_0.

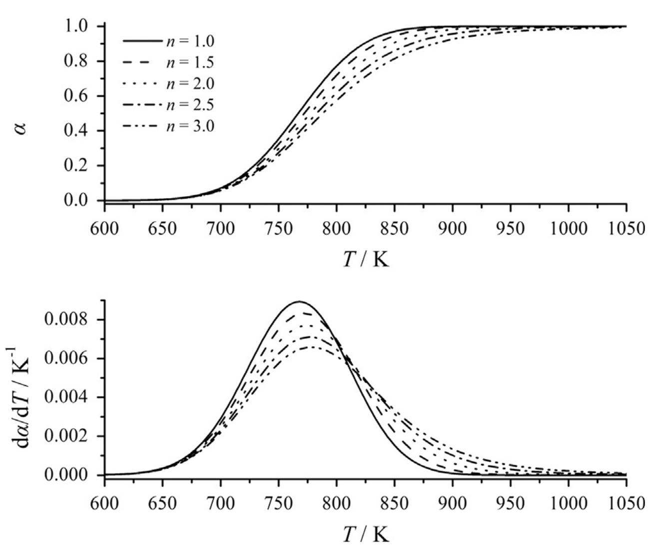

Fig. 2. The simulated $\alpha-T$ and dα/d$T-T$ curves of the Gaussian DAEM processes with the following parameters: $A=1.67\times10^{13}$ s^{-1}, $E_0=228$ kJ mol^{-1}, $\beta=10$ K min^{-1}, $\sigma=5.0\%$ E_0, and $n=1.0$, 1.5, 2.0, 2.5 and 3.0.

5. Parameter estimation methods

The DAEM has some mathematical difficulties in parameter estimation because of the complex structure of the DAEM equation [28]. The parameter estimation methods for the DAEM can be classified as distribution-free and distribution-fitting methods. Miura and his colleague [42,43] proposed the differential and integral methods to estimate $f(E)$ in the DAEM without previous assumptions for $f(E)$ in 1995 and 1998, respectively. In further discussion, they are referred to as the Miura differential method and the Miura–Maki integral method [6], which are distribution-free methods. The previous assumption for $f(E)$ is required in the use of the distribution-fitting methods, which are based on some direct search optimization methods.

5.1. Distribution-free methods

The assumptions and detailed derivation processes of the Miura differential method and the Miura–Maki integral method can be found in the literature [42,43]. The procedures for calculating $f(E)$ by using these distribution-free methods are compared in Table 1. From Table 1, it can be obtained that the $\alpha-T$ data at different heating rates are required in the use of the Miura–Maki integral method, while the Miura differential method employs instantaneous $\alpha-T$ and dα/d$T-T$ data. Therefore, for the Miura differential method, it is more sensitive to experimental noise.

To evaluate the validity of the Miura differential method and the Miura–Maki integral method, it is examine to see if $f(E)$ determined from the $\alpha-T$ and dα/d$T-T$ data constructed from known sets of DAEM parameters is consistent with the assumed

Table 2
DAEM parameters of cellulose, hemicellulose and lignin presented in the literature [25].

Material	E_0 (kJ mol^{-1})	σ (kJ mol^{-1})	A (s^{-1})
Hemicellulose	175.6	4.3	$10^{14.52}$
Cellulose	185.4	3.5	$10^{13.64}$
Lignin	195.4	32.0	$10^{13.98}$

Table 1
Comparison between the Miura differential method and the Miura–Maki integral method to estimate $f(E)$.

Step	The Miura differential method	The Miura–Maki integral method
1	Obtain α versus T and dα/dT versus T relationships at three heating rates at least	Obtain α versus T relationships at three heating rates at least
2	Calculate the values of $\ln[(\mathrm{d}\alpha/\mathrm{d}T)/(1-\alpha)]$ at selected α values for different heating rates	Calculate the values of $\ln(\beta/T^2)$ at selected α values for different heating rates
3	Plot $\ln[(\mathrm{d}\alpha/\mathrm{d}T)/(1-\alpha)]$ versus $1/T$ at selected α values, and determine E	Plot $\ln(\beta/T^2)$ versus $1/T$ at selectedα values, and determine E
4	Plot α versus E, and differentiate α versus E relationship to obtain $f(E)$	Plot α versus E, and differentiate α versus E relationship to obtain $f(E)$

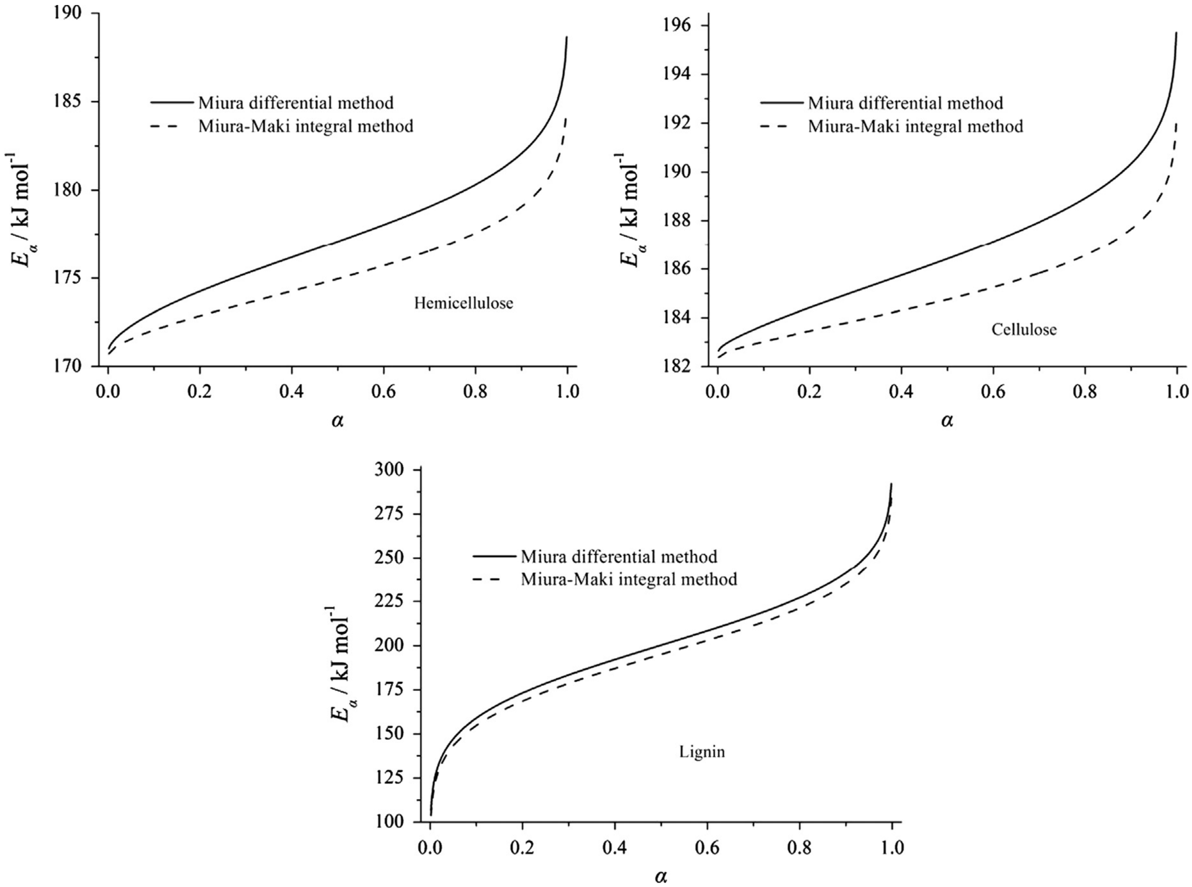

Fig. 3. The activation energy values as a function of conversion for the pyrolysis of hemicellulose, cellulose and lignin.

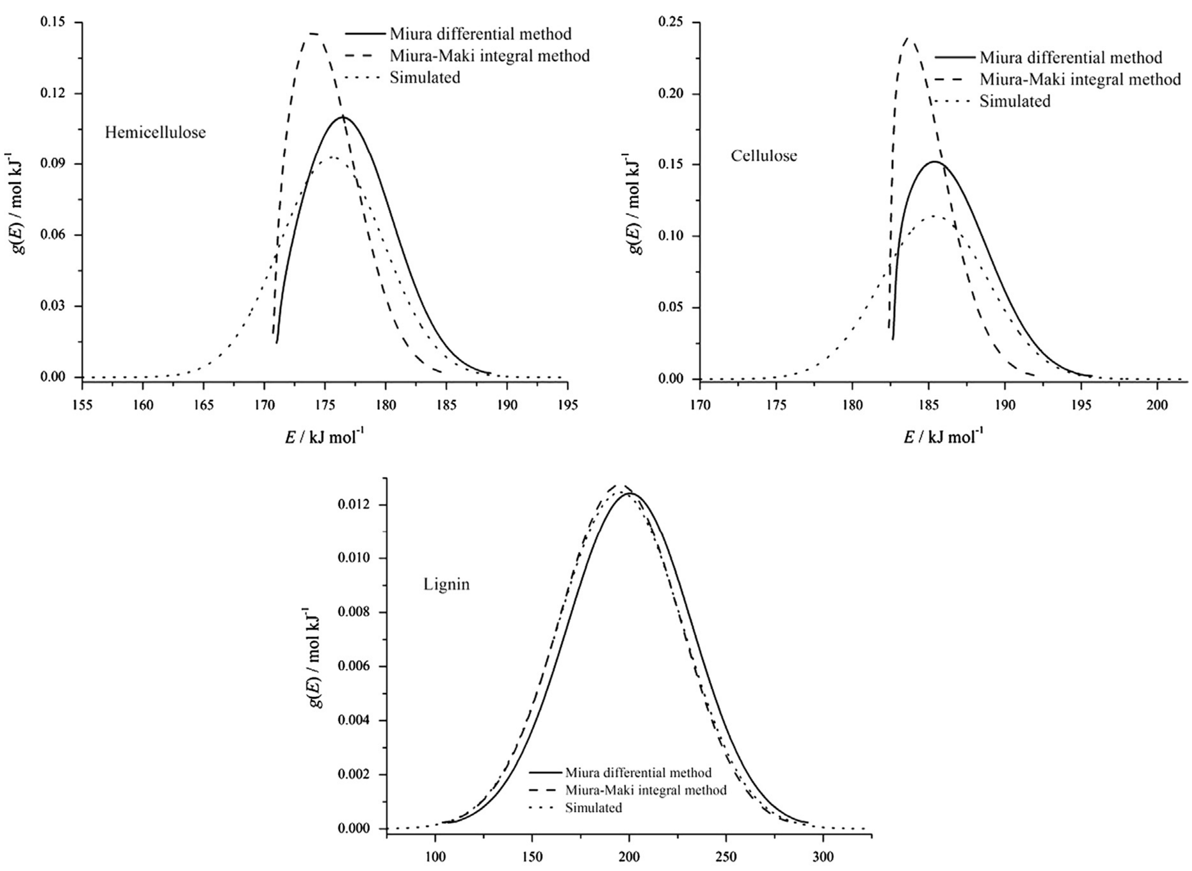

Fig. 4. Comparison of the assumed $f(E)$ and the $f(E)$ estimated by the Miura differential method and the Miura–Maki integral method.

Table 3
Different sets of kinetic parameters of the first-order Gaussian DAEM for cellulose pyrolysis.

Set of kinetic parameters	A (s^{-1})	E_0 (kJ mol^{-1})	σ (kJ mol^{-1})	SSR
1	5.5472×10^{11}	161.8438	4.3217	0.012030
2	6.3165×10^{13}	185.1297	4.5979	0.002649
3	1.0107×10^{14}	187.4462	4.5818	0.002569
4	9.9504×10^{14}	198.7059	5.2204	0.003468
5	1.0004×10^{16}	210.0828	5.8349	0.004290
6	9.8514×10^{17}	232.7228	6.9938	0.005719

one. For this purpose, some simulated DAEM processes are considered.

In the literature [25], the first-order Gaussian DAEM was used to successfully describe the pyrolysis kinetics of hemicellulose, cellulose and lignin, which are three main components of lignocellulosic biomass. Their parameters are employed to construct the simulated DAEM processes, as shown in Table 2.

Fig. 3 shows the activation energy values as a function of conversion for the pyrolysis of hemicellulose, cellulose and lignin. From Fig. 3, it can be observed that the activation energies significantly increase with increasing conversion. Differentiating

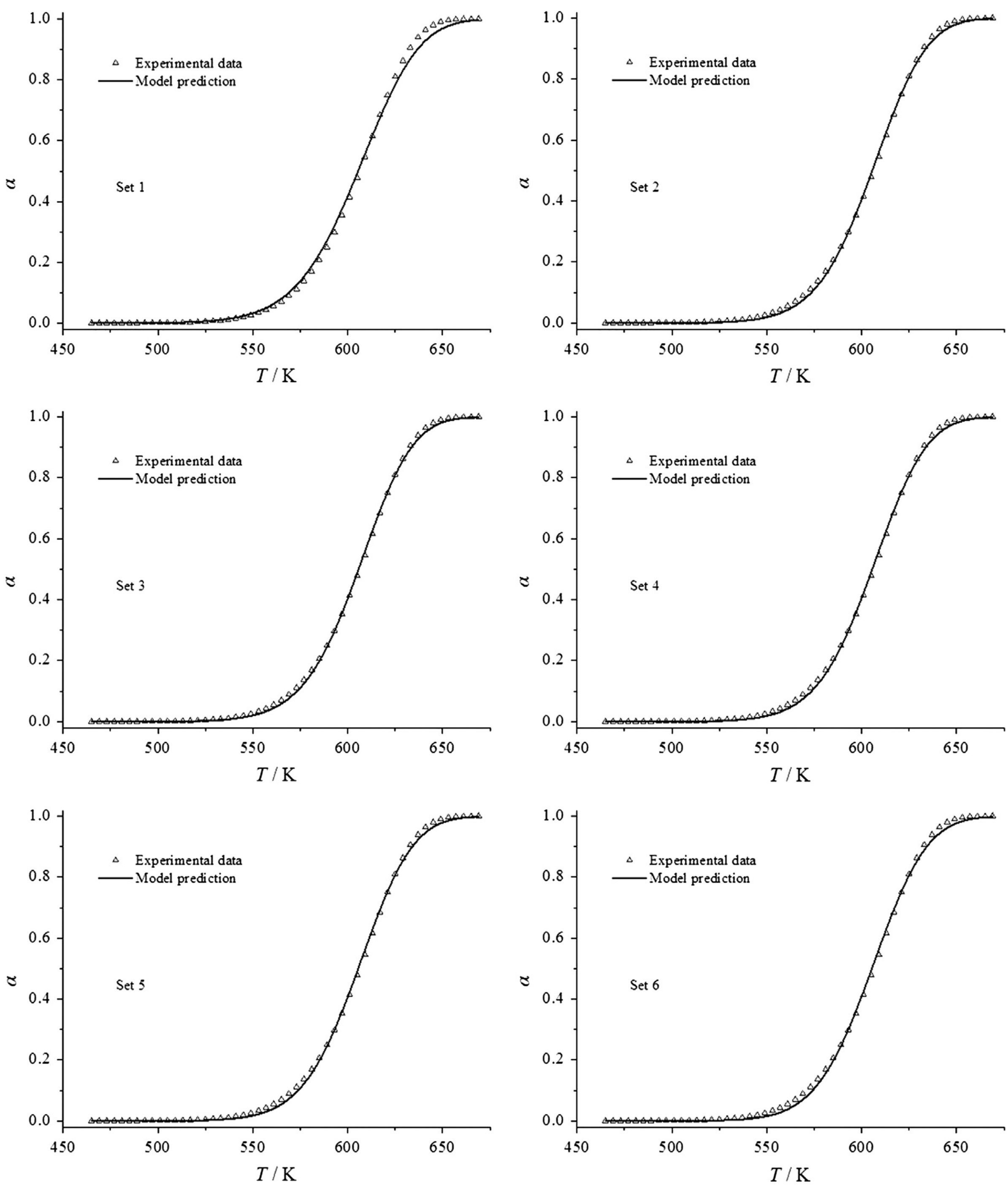

Fig. 5. Multiplicity in kinetic parameters of the first-order Gaussian DAEM for cellulose pyrolysis.

the α versus E relationships gives $f(E)$ curves, which are shown in Fig. 4 with the pre-assumed Gaussian distributions. The estimated activation energy distributions are close with the assumed distribution for lignin. However, the errors involved in the activation energy distributions obtained from the Miura differential method and the Miura–Maki integral method are significant for hemicellulose and cellulose. Therefore, the validity of the Miura differential method and the Miura–Maki integral method for the estimation of the DAEM kinetic parameters should be systematically investigated.

5.2. Distribution-fitting methods

The conventional procedures of the distribution-fitting methods for the determination of the kinetic parameters of DAEM include four steps

(1) A is assumed to be an unknown constant, or is directly assigned to a given constant, or A is equaled to A_0T^m;
(2) $f(E)$ is assumed to be a Gaussian or another distribution;
(3) The following objective function is constructed

$$SSR = \sum_{i=1}^{n_d} (\alpha_{\exp,i} - \alpha_{\mathrm{cal},i})^2 \tag{27}$$

where $\alpha_{\exp}$ and α_{cal} are experimental and calculated values of conversion, respectively;
(4) A and $f(E)$ are obtained by minimizing the objective function (27).

In the literature, the grid search method [19,44], genetic algorithm [45], pattern search method [46], Multistart algorithm [47], Hook-Jeeves method [48], and simulated annealing optimization method [28] were usually used for minimizing Eq. (27).

The disadvantage of the distribution-fitting methods is that different sets of DAEM kinetic parameters provide an approximately equally good fit to experimental data at a single heating rate [25,49]. To demonstrate the existence of multiplicity in DAEM kinetic parameters, the experimental data (52 data points) of cellulose pyrolysis at a heating rate of 10 K min^{-1} is used. The Gaussian distribution of first-order reactions is employed to analyze the experimental data of cellulose pyrolysis. Parameter estimation is performed by means of the pattern search method. Several sets of parameters is obtained with different initial guesses and listed in Table 3. The results from the first-order Gaussian DAEMs with different sets of kinetic parameters are shown in Fig. 5, where it can be seen that the DAEMs compare very well with the experimental data. Fig. 6 shows the relationship between the multiple sets of the mean value (E_0) of the activation energy distribution and the corresponding frequency factor (A). A perfect linear relationship can be obtained between ln$A$ and E_0

$$\ln A = 28.61335 + 4.92587E_0 \tag{28}$$

where A and E_0 are expressed in s^{-1} and kJ mol^{-1}, respectively. This kind multiplicity of the DAEM kinetic parameters was studied in detail in the literature [12,49]. Therefore, the use of the method involving nonlinear least squares optimization of multiple heating rate data is expected to result in unique kinetic parameters [50].

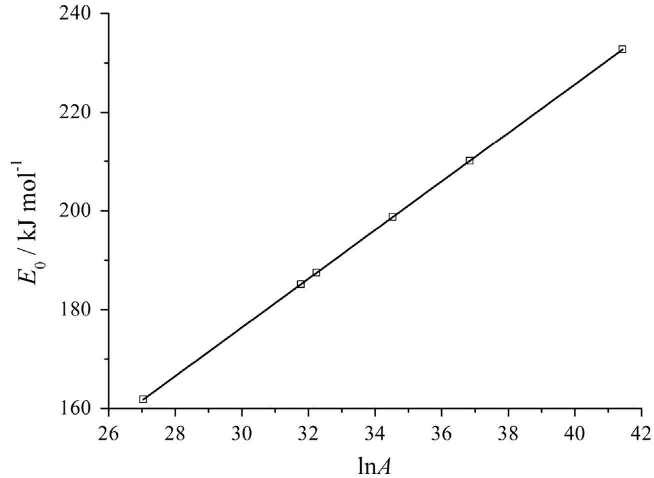

Fig. 6. The relationship between E_0 and ln$A$ for multiple sets of kinetic parameters. The solid line represents the linear fitting. (A is expressed in s^{-1}).

6. DAEM for lignocellulosic biomass pyrolysis kinetics

Lignocellulosic biomass consists of three major components (i.e. cellulose, hemicellulose, and lignin) and also contains a variety of minor components (i.e. inorganic matters) [51]. Cellulose, hemicellulose, and lignin are all long-chain biopolymers [52,53]. There are a lot of reactions involved in the thermal decomposition of cellulose, hemicellulose, and lignin. Therefore, it is not accurate enough to describe the entire pyrolysis processes of them with a single reaction [54]. In fact, the pyrolysis of a biomass component requires a range of activation energies that vary with the size of the polymer and the location of the bonds that are being broken [55]. Therefore, the DAEM has been used previously to describe the pyrolysis of biomass components [23,55–60].

In general, the conversion rate curve (i.e. the $d\alpha/dT - T$ curve) of the pyrolysis of lignocellulosic biomass shows a peak and a peak shoulder on the left side of the peak [5]. However, according to the numerical results of the DAEM processes [29,39,41,61,62], the conversion rate curves of the DAEM with a certain activation energy distribution (i.e. Gaussian, Weibull, Logistic distributions) and certain frequency factor (i.e. A=constant, $A=A_0T^m$, $A=e^{a+bE_0}$) show one single peak and no peak shoulder. Thus, it is impossible to describe the entire pyrolysis process of lignocellulosic biomass with such the DAEM. Some researchers reported that they used the DAEM to describe the pyrolysis kinetics of lignocellulosic biomass based on the Miura–Maki integral method [63–67]. However, they only obtained some values of E_α and A_α or the ranges of E and A in a certain range of conversion. $f(E)$ was supposed to be given by numerical differentiating the α versus E_α relationship. However, sometimes there were several points in their obtained $\alpha - E_\alpha$ plot, sometimes α varied with E_α dramatically. In those situations, it is difficult to get the derivatives of the α versus E_α relationship.

Since the pyrolysis kinetics of biomass components can be described well by using the single DAEM, some comprehensive models consisting of two or three parallel DAEM reactions were proposed to describe the overall decomposition kinetics of lignocellulosic biomass [25,54,55,68]. In those models, the lignocellulosic biomass was regarded as a sum of several pseudocomponents. It was further assumed that there was no interaction among these pseudocomponents and the pyrolysis of each pseudocomponent would be described by using a single first-order Gaussian DAEM.

$$\alpha(t) = \frac{\sum_{i=1}^{M} c_i \alpha_i(t)}{\sum_{i=1}^{M} c_i} \tag{29}$$

$$\frac{d\alpha}{dt} = \frac{\sum_{i=1}^{M} c_i (d\alpha_i/dt)}{\sum_{i=1}^{M} c_i} \tag{30}$$

$$\alpha_i(t) = 1 - \frac{1}{\sigma_i\sqrt{2\pi}} \int_0^\infty \exp\left[-\int_0^t A_i \exp\left(-\frac{E}{RT}\right) dt - \frac{(E-E_{0i})^2}{2\sigma_i^2} \right] dE \tag{31}$$

Table 4
Summary of DAEM for lignocellulosic biomass pyrolysis kinetics.

Biomass	Experimental method and condition	Model	Parameter estimation method	Kinetic parameters	References
Jerusalem artichoke tubers	Thermogravimetric analysis—linear heating: 5, 10, 20 and 30 K min^{-1}; inert atmosphere: nitrogen	The first-order DAEM	The Miura–Maki integral method	E: 152–232.5 kJ mol^{-1} A: 2.93 × 10^{11}–7.97 × 10^{23} s^{-1}	[66]
Pine pellets	Thermogravimetric analysis—linear heating: 10, 15, and 20 K min^{-1}; inert atmosphere: nitrogen	The first-order DAEM	The Miura–Maki integral method	E: 160–270 kJ mol^{-1} A: 10^{11}–10^{16} s^{-1}	[67]
Sugarcane trash sugarcane bagasse pine sawdust Cedar sawdust coffee residue	Thermogravimetric analysis (sugarcane trash, sugarcane bagasse, pine sawdust, cedar sawdust, coffee residue)—linear heating: 0.0833–1 K s^{-1}; inert atmosphere: nitrogen	The first-order DAEM	The Miura–Maki integral method	Sugarcane trash E: 110–320 kJ mol^{-1} Sugarcane bagasse E: 110–320 kJ mol^{-1} Pine sawdust E: 200–350 kJ mol^{-1} Cedar sawdust E: 120–315 kJ mol^{-1}	[63]
Xylan Microcrystalline cellulose	Thermogravimetric analysis—linear heating: 5 K min^{-1}; inert atmosphere: helium	The first-order Gaussian DAEM	Distribution-fitting method: pattern search method	Xylan— E_0=178.311 kJ mol^{-1}, σ=5.848 kJ mol^{-1}, $A=10^{12.702}$ s^{-1} Cellulose— E_0=210.037 kJ mol^{-1}, σ=0.944 kJ mol^{-1}, $A=10^{13.904}$ s^{-1}	[55]
Indulin AT lignin Lignoboost™ lignin Acetocell lignin	Thermogravimetric analysis—linear heating: 5, 10, and 15 K min^{-1} for indulin AT lignin, 5, 15, and 40 K min^{-1} for Lignoboost™ and acetocell lignin; inert atmosphere: nitrogen	The first-order Gaussian DAEM	The Miura–Maki integral method	Indulin AT lignin: E_0=192 kJ mol^{-1}, σ=43 kJ mol^{-1}, $A=10^{13}$ s^{-1} Lignoboost™ lignin: E_0=193 kJ mol^{-1}, σ=37 kJ mol^{-1}, $A=10^{13}$ s^{-1} Acetocell lignin: E_0=193 kJ mol^{-1}, σ=47 kJ mol^{-1}, $A=10^{13}$ s^{-1}	[58]
Alcell lignin	Thermogravimetric analysis—linear heating: 5, 10 and 15 K min^{-1}; inert atmosphere: nitrogen	The first-order DAEM	Miura–Maki integral method	Alcell lignin—E: 129–361 kJ mol^{-1}, A: 6.2 × 10^{11}–9.2 × 10^{22} s^{-1}, E_0=254.3 kJ mol^{-1}, σ=29.0 kJ mol^{-1}	[57]
Kraft lignin	Fixed-bed reactor—linear heating rates: 5, 10 and 15 K min^{-1}; inert atmosphere: helium			Kraft lignin—E: 80–158 kJ mol^{-1}, A: 3.3 × 10^{7}–1.84 × 10^{9} s^{-1}, E_0=123.0 kJ mol^{-1}, σ=11.0 kJ mol^{-1}	
Alcell lignin	Thermogravimetric analysis—linear heating: 5, 10, and 15 K min^{-1}; inert atmosphere: nitrogen	The first-order Gaussian DAEM with $A=A_0T^m$	Distribution-fitting method: simulated annealing optimization method	E_0=135 kJ mol^{-1} σ=33 kJ mol^{-1} m=2.8 A_0=92670 min^{-1} K^{-1}	[28]
Hemicellulose Cellulose Lignin Wood	Thermogravimetric analysis—linear heating: 5 K min^{-1}; inert atmosphere: nitrogen	The first-order Gaussian DAEM	Distribution-fitting method	Hemicellulose— E_0=132.9 kJ mol^{-1}, σ=2.4 kJ mol^{-1}, A=1.25 × 10^{10} s^{-1} Cellulose— E_0=175.6 kJ mol^{-1}, σ=0.4 kJ mol^{-1}, A=3.41 × 10^{12} s^{-1} Lignin— E_0=101.0 kJ mol^{-1}, σ=11.3 kJ mol^{-1}, A=2.22 × 10^{6} s^{-1} Wood— E_0=123.52 kJ mol^{-1}, σ=5.97 kJ mol^{-1}, A=1.57 × 10^{8} s^{-1}	[56]
Fresh water algae	Thermogravimetric analysis—linear heating: 5 and 10 K min^{-1}; inter atmosphere	The nth-order Gaussian DAEM	Distribution-fitting method: Multistart algorithm	5 K min^{-1}: E_0=189.15 kJ mol^{-1}, σ=14.73 kJ mol^{-1}, A=1.1291 × 10^{16} s^{-1}, n=7.88 10 K min^{-1}: E_0=190.02 kJ mol^{-1}, σ=14.73 kJ mol^{-1},	[47]

Table 4 (*continued*)

Biomass	Experimental method and condition	Model	Parameter estimation method	Kinetic parameters	References
Cellulose	Thermogravimetric analysis—linear heating: 5, 25, and 50 K min^{-1}; inert atmosphere: nitrogen	The *n*th-order Logistic DAEM	Distribution-fitting method: pattern search method	$A=2.6021\times10^{16}$ s^{-1}, $n=6.63$ $\mu=258.5718$ kJ mol^{-1} $\sigma=2.6601$ kJ mol^{-1} $A=1.6218\times10^{17}$ s^{-1} $n=1.1101$	[23]
Corn stalk skin	Thermogravimetric analysis—Linear heating: 20, 35, 50, 75, and 100 K min^{-1}; Inert atmosphere: nitrogen	The first-order DAEM	The Miura–Maki integral method	E: 62–169 kJ mol^{-1} A: $10^{10.8}$–$10^{26.5}$ s^{-1}	[65]
Rice straw Rice husk Corncob	Thermogravimetric analysis—linear heating: 2, 5 and 10 K min^{-1}; inert atmosphere: nitrogen	The first-order DAEM	The Miura–Maki integral method	Rice straw—E: 118–208 kJ mol^{-1} f(E) peaks at 170 kJ mol^{-1} Rice husk—E: 150–224 kJ mol^{-1} f(E) peaks at 174 kJ mol^{-1} Corncob—E: 140–229 kJ mol^{-1} f(E) peaks at 183 kJ mol^{-1}	[64]
Sawdust	Thermogravimetric analysis—linear heating: 5, 10, 15, and 20 K min^{-1}; atmosphere: hydrogen or syngas (H_2: 68.1%, CO: 30.1%, C_1–C_4: 0.9%, CO_2: 0.9%)	The first-order DAEM	The Miura–Maki integral method	E: 161.9–202.3 kJ mol^{-1} A: 4.8×10^5–4.5×10^{13} s^{-1}	[69]
Wheat straw Winter barley straw Oat straw	Thermogravimetric analysis—linear heating: 11, 22, and 47 K min^{-1}; inert atmosphere: nitrogen	Two parallel first-order Gaussian DAEM reactions $-\mathrm{d}m/\mathrm{d}t=c_1\mathrm{d}\alpha_1/\mathrm{d}t+c_2\mathrm{d}\alpha_2/\mathrm{d}t$ where α_1 and α_2 are described by the first-order Gaussian DAEM	Distribution-fitting method	See Table 4.1	[68]
Corn stalk Rice husk Sorghum straw Wheat straw	Thermogravimetric analysis—linear heating: 4 and 40 K min^{-1} (corn stalk, rice husk, sorghum straw, and wheat straw); stepwise program: 20 K min^{-1} with steps at 250, 300, 350, and 400 °C, 20 K min^{-1} with steps at 225, 275, 325, and 375 °C for corn stalk, sorghum straw and wheat straw; 20 K min^{-1} with steps at 225, 275, 325, 375, and 425 °C, 20 K min^{-1} with steps at 200, 250, 300, 350, and 400 °C for rice husk; Inert atmosphere: argon	Three parallel first-order DAEM reactions $-\mathrm{d}m/\mathrm{d}t=\sum_{i=1}^{3}c_i\mathrm{d}\alpha_i/\mathrm{d}t$ where c_j is the amount of volatiles formed from a unit mass of pseudocomponent j; α_j is described by the first-order Gaussian DAEM.	Distribution-fitting method	See Table 4.2	[25]
Corn stover Cotton stalk Palm oil husk Pine wood Red oak Sugarcane bagasse Switchgrass Wheat straw	Thermogravimetric analysis—linear heating: 5 and 20 K min^{-1}; inert atmosphere: helium	Three parallel first-order DAEM reactions $-\mathrm{d}m/\mathrm{d}t=\sum_{i=1}^{3}c_i\mathrm{d}\alpha_i/\mathrm{d}t$ where c_j is the amount of volatiles formed from a unit mass of pseudocomponent j; α_j is described by the first-order Gaussian DAEM	Distribution-fitting method: pattern search method	See Table 4.3	[55]

Table 4.1
Kinetic parameters of lignocellulosic biomass pyrolysis in the literature [68].

	Wheat straw	Winter barley straw	Oat straw
E_{01} (kJ mol^{-1})	167.3	167.3	167.3
E_{02} (kJ mol^{-1})	225.7	225.7	225.7
σ_1 (kJ mol^{-1})	1.8	1.8	1.8
σ_2 (kJ mol^{-1})	25.9	25.9	25.9
A_1 (s^{-1})	$10^{12.53}$	$10^{12.91}$	$10^{12.21}$
A_2 (s^{-1})	$10^{17.78}$	$10^{18.14}$	$10^{17.90}$
c_1	0.36	0.31	0.26
c_2	0.35	0.36	0.47

where the weight factor c_i is equal to the amount of volatiles formed from the ith pseudocomponent, and M is the number of pseudocomponents.

It is noted that a pseudocomponent represents the totality of those decomposing species that can be described by the same kinetic parameters. Those pseudocomponents are usually linked the real biomass components. In particular, for the three-parallel-DAEM-reaction model [25,55], the first and second pseudocomponents represent the fractions of hemicellulose and cellulose that react at low temperature, and the third pseudocomponent represents the sum of the remaining amounts of hemicellulose and cellulose plus the fractions of lignin.

By following the above stepwise discussion, the research and development efforts in the literature on the DAEM for lignocellulosic biomass pyrolysis are summarized in Table 4. Most kinetic studies of lignocellulosic biomass pyrolysis have been made using thermogravimetric analysis (TGA) at relatively slow heating rates. In the tabulated summary, the elemental composition of lignocellulosic biomass sample, the experimental methods and conditions are highlighted. The resultant DAEM kinetic parameters together with the parameter estimation methods are also provided. The efforts on DAEM for the pyrolysis of lignocellulosic biomass indicate that the model consisting of three parallel DAEM

Table 4.2
Kinetic parameters of lignocellulosic biomass pyrolysis in the literature [25].

	Corn stalk	Sorghum straw	Rice husk	Wheat straw
E_{01} (kJ mol^{-1})	176	176	176	176
E_{02} (kJ mol^{-1})	185	185	185	185
E_{03} (kJ mol^{-1})	189	189	189	189
σ_1 (kJ mol^{-1})	7.1	7.1	7.1	7.1
σ_2 (kJ mol^{-1})	1.7	1.7	1.7	1.7
σ_3 (kJ mol^{-1})	32.7	32.7	32.7	32.7
A_1 (s^{-1})	$10^{14.13}$	$10^{14.13}$	$10^{14.13}$	$10^{14.13}$
A_2 (s^{-1})	$10^{13.71}$	$10^{13.71}$	$10^{13.71}$	$10^{13.71}$
A_3 (s^{-1})	$10^{13.90}$	$10^{13.90}$	$10^{13.90}$	$10^{13.90}$
c_1	0.14	0.10	0.08	0.16
c_2	0.25	0.23	0.36	0.38
c_3	0.31	0.34	0.33	0.19

Table 4.3
Kinetic parameters of lignocellulosic biomass pyrolysis in the literature [55].

	Corn stover	Cotton stalk	Palm oil husk	Pine wood	Red oak	Sugarcane bagasse	Switchgrass	Wheat straw
E_{01} (kJ mol^{-1})	179.602	178.188	169.710	186.701	183.109	184.750	186.776	175.506
E_{02} (kJ mol^{-1})	207.381	205.287	199.966	214.364	209.58	212.483	212.057	204.244
E_{03} (kJ mol^{-1})	239.344	239.463	236.110	271.758	242.145	234.759	260.952	240.610
σ_1 (kJ mol^{-1})	5.888	5.591	5.147	8.769	8.342	5.419	4.586	5.375
σ_2 (kJ mol^{-1})	1.174	1.789	1.313	1.126	0.706	1.339	1.361	1.130
σ_3 (kJ mol^{-1})	31.414	41.767	39.998	29.250	26.583	36.493	39.293	38.422
A_1 (s^{-1})	$10^{13.007}$	$10^{13.132}$	$10^{12.699}$	$10^{13.006}$	$10^{13.007}$	$10^{13.007}$	$10^{13.007}$	$10^{12.700}$
A_2 (s^{-1})	$10^{13.949}$	$10^{13.800}$	$10^{13.618}$	$10^{13.803}$	$10^{13.618}$	$10^{13.805}$	$10^{13.804}$	$10^{13.800}$
A_3 (s^{-1})	$10^{16.003}$	$10^{15.738}$	$10^{15.953}$	$10^{16.399}$	$10^{15.006}$	$10^{15.769}$	$10^{16.536}$	$10^{15.812}$
c_1	0.16337	0.12999	0.10116	0.32147	0.27282	0.22009	0.23651	0.15916
c_2	0.25386	0.35824	0.32121	0.38557	0.37320	0.35035	0.33376	0.28027
c_3	0.16481	0.20008	0.19241	0.08412	0.12204	0.12289	0.20159	0.23410

reactions is the most accurate and up-to-date approach for modeling the pyrolysis kinetics of lignocellulosic biomass.

7. Summaries

The pyrolysis of lignocellulosic biomass involves many reactions, which can't be well described by a simple single kinetic model. In the literature, the DAEM was usually used to describe its pyrolysis kinetics. This review presents a state-of-the-art review of the DAEM for lignocellulosic biomass pyrolysis. This review starts with the derivation of the DAEM and a brief overview of the activation energy distribution and frequency factor in the DAEM. Then the parameter estimation methods for the determination of the DAEM kinetic parameters are critically studied. The final part is the overview of the application of the DAEM to lignocellulosic biomass pyrolysis. A handy, up-to-date overview of the existing research and developments efforts and major findings in the DAEM for lignocellulosic biomass pyrolysis is provided. It is hoped that this review is critical for helping understand the application of the DAEM in the thermal decomposition of other degradable materials.

Acknowledgements

The authors would like to acknowledge financial support from the National Natural Science Foundation of China (Grant number: 50806048), State Key Laboratory of Heavy Oil Processing, China University of Petroleum (Grant number: 2012-1-02), and School of Agriculture and Biology, Shanghai Jiao Tong University (Grant number: NRC201101). Ronghou Liu was supported by the National Natural Science Foundation of China (Grant no. 51176121). The authors would like to acknowledge Le Zhang, a master degree candidate from School of Agriculture and Biology, Shanghai Jiao Tong University, for his help on English grammar check.

References

[1] Mohan D, Pittman CU, Steele PH. Pyrolysis of wood/biomass for bio-oil: a critical review. Energy Fuels 2006;20:848–89.
[2] Huber GW, Iborra S, Corma A. Synthesis of transportation fuels from biomass: chemistry, catalysts, and engineering. Chem Rev 2006;106:4044–98.
[3] Papadikis K, Gu S, Bridgwater AV, Gerhauser H. Application of CFD to model fast pyrolysis of biomass. Fuel Process Technol 2009;90:504–12.
[4] Saddawi A, Jones JM, Williams A, Wójtowicz MA. Kinetics of the thermal decomposition of biomass. Energy Fuels 2010;24:1274–82.
[5] White JE, Catallo WJ, Legendre BL. Biomass pyrolysis kinetics: a comparative critical review with relevant agricultural residue case studies. J Anal Appl Pyrolysis 2011;91:1–33.
[6] Cai J, Li T, Liu R. A critical study of the Miura–Maki integral method for the estimation of the kinetic parameters of the distributed activation energy model. Bioresour Technol 2011;102:3894–9.
[7] Navarro MV, Aranda A, Garcia T, Murillo R, Mastral AM. Application of the distributed activation energy model to blends devolatilisation. Chem Eng J 2008;142:87–94.
[8] Güneş M, Güneş SK. Distributed activation energy model parameters of some Turkish coals. Energy Sources Part A 2008;30:1460–72.
[9] Caprariis B, Filippis P, Herce C, Verdone N. Double-Gaussian distributed activation energy model for coal devolatilization. Energy Fuels 2012;26:6153–9.
[10] Dawood A, Miura K. Pyrolysis kinetics of γ-irradiated polypropylene. Polym Degrad Stab 2001;73:347–54.
[11] Yan JH, Zhu HM, Jiang XG, Chi Y, Cen KF. Analysis of volatile species kinetics during typical medical waste materials pyrolysis using a distributed activation energy model. J Hazard Mater 2009;162:646–51.
[12] Campbell JH, Koskinas GJ, Gregg M. Gas evolution during oil shale pyrolysis 2. Kinetic analsis. Fuel 1980;57:377–83.
[13] Tiwari P, Deo M. Detailed kinetic analysis of oil shale pyrolysis TGA data. AIChE J 2012;58:505–15.
[14] Vand V. A theory of the irreversible electric resistance changes of metallic films evaporated in vacuum. Proc Phys Soc London 1943;A55:222–46.

[15] Pitt GJ. The kinetics of the evolution of volatile products from coal. Fuel 1962;41:267–74.
[16] Anthony DB, Howard JB. Coal devolatilization and hydrogasification. AIChE J 1976;22:625–56.
[17] Vyazovkin S, Burnham AK, Criado JM, Perez-Maqueda LA, Popescu C, Sbirrazzuoli N. ICTAC Kinetics Committee recommendations for performing kinetic computations on thermal analysis data. Thermochim Acta 2011;520:1–19.
[18] Burnham AK, Braun RL. Global kinetic analysis of complex materials. Energy Fuels 1999;13:1–22.
[19] Lakshmanan CC, White N. A new distributed activation-energy model using Weibull distribution for the representation of complex kinetics. Energy Fuels 1994;8:1158–67.
[20] Cai JM, Liu R. Weibull mixture model for modeling nonisothermal kinetics of thermally stimulated solid-state reactions: application to simulated and real kinetic conversion data. J Phys Chem B 2007;111:10681–6.
[21] Burnham AK, Weese RK, Weeks BL. A distributed activation energy model of thermodynamically inhibited nucleation and growth reactions and its application to the β-δ phase transition of HMX. J. Phys. Chem. B 2004;108:19432–41.
[22] Cai JM, Jin C, Yang SY, Chen Y. Logistic distributed activation energy model—Part 1: Derivation and numerical parametric study. Bioresour Technol 2011;102:1556–61.
[23] Cai JM, Yang SY, Li T. Logistic distributed activation energy model—Part 2: Application to cellulose pyrolysis. Bioresour Technol 2011;102:3642–4.
[24] Fiori L, Valbusa M, Lorenzi D, Fambri L. Modeling of the devolatilization kinetics during pyrolysis of grape residues. Bioresour Technol 2012;103:389–97.
[25] Várhegyi G, Bobaly B, Jakab E, Chen HG. Thermogravimetric study of biomass pyrolysis kinetics. A distributed activation energy model with prediction tests. Energy Fuels 2011;25:24–32.
[26] Deng C, Cai J, Liu R. Kinetic analysis of solid-state reactions: evaluation of approximations to temperature integral and their applications. Solid State Sci 2009;11:1375–9.
[27] Cai JM, Yao FS, Yi WM, He F. New temperature integral approximation for nonisothermal kinetics. AIChE J 2006;52:1554–7.
[28] Mani T, Murugan P, Mahinpey N. Determination of distributed activation energy model kinetic parameters using simulated annealing optimization method for nonisothermal pyrolysis of lignin. Ind Eng Chem Res 2009;48:1464–7.
[29] Cai JM, Liu RH. New distributed activation energy model: numerical solution and application to pyrolysis kinetics of some types of biomass. Bioresour Technol 2008;99:2795–9.
[30] Cai JM, Liu RH. New approximation for the general temperature integral. J Therm Anal Calorim 2007;90:469–74.
[31] L'vov BV, Galwey AK. Interpretation of the kinetic compensation effect in heterogeneous reactions: thermochemical approach. Int Rev Phys Chem 2013;32:515–57.
[32] Miura K, Maki T. Simplified method to estimate $f(E)$ in distributed activation energy model for analyzing coal pyrolysis reaction. J Chem Eng Jpn 1998;31:228–35.
[33] Nikolaev AV, Logvinenko VA, Gorbatchev VM. Special features of the compensation effect in non-isothermal kinetics of solid-phase reactions. J Therm Anal 1974;6:473–7.
[34] Suuberg EM. Approximate solution technique for non-isothermal, Gaussian distributed activation-energy models. Combust Flame 1983;50:243–6.
[35] Du ZY, Sarofim AF, Longwell JP. Activation-energy distribution in temperature-programmed desorption – modeling and application to the soot – oxygen system. Energy Fuels 1990;4:296–302.
[36] Donskoi E, McElwain DLS. Optimization of coal pyrolysis modeling. Combust Flame 2000;122:359–67.
[37] Rostami AA, Hajaligol MR, Wrenn SE. A biomass pyrolysis sub-model for CFD applications. Fuel 2004;83:1519–25.
[38] Braun RL, Burnham AK. Analysis of chemical-reaction kinetics using a distribution of activation-energies and simpler models. Energy Fuels 1987;1:153–61.
[39] Güneş M, Güneş SK. The influences of various parameters on the numerical solution of nonisothermal DAEM equation. Thermochim Acta 1999;336:93–6.
[40] Órfão JJM. Review and evaluation of the approximations to the temperature integral. AIChE J 2007;53:2905–15.
[41] Cai JM, He F, Yao FS. Nonisothermal nth-order DAEM equation and its parametric study—use in the kinetic analysis of biomass pyrolysis. J Math Chem 2007;42:949–56.
[42] Miura K, Maki T. A simple method for estimating $f(E)$ and $k_0(E)$ in the distributed activation energy model. Energy Fuels 1998;12:864–9.
[43] Miura K. A new and simple method to estimate $f(E)$ and $k_0(E)$ in the distributed activation energy model from three sets of experimental data. Energy Fuels 1995;9:302–7.
[44] Güneş M, Güneş SK. A direct search method for determination of DAEM kinetic parameters from nonisothermal TGA data (note). Appl Math Comput 2002;130:619–28.
[45] Dhumal SS, Saha RK. Application of genetic algorithm for evaluation of kinetic parameters of coal pyrolysis. J Energy Environ 2006;5:112–24.
[46] Cai J, Ji L. Pattern search method for determination of DAEM kinetic parameters from nonisothermal TGA data of biomass. J Math Chem 2007;42:547–53.
[47] Kirtania K, Bhattacharya S. Application of the distributed activation energy model to the kinetic study of pyrolysis of the fresh water algae Chlorococcum humicola. Bioresour Technol 2012;107:476–81.
[48] Várhegyi G, Sebestyen Z, Czegeny Z, lezsovits F, Konczol S. Combustion kinetics of biomass materials in the kinetic regime. Energy Fuels 2012;26:1323–35.
[49] Lakshmanan CC, Bennett ML, White N. Implications of multiplicity in kinetic parameters to petroleum exploration: distributed activation energy models. Energy Fuels 1991;5:110–7.
[50] Aboyade AO, Carrier M, Meyer EL, Knoetze JH, Gorgens JF. Model fitting kinetic analysis and characterisation of the devolatilization of coal blends with corn and sugarcane residues. Thermochim Acta 2012;530:95–106.
[51] Yin CG. Microwave-assisted pyrolysis of biomass for liquid biofuels production. Bioresour Technol 2012;120:273–84.
[52] Klemm D. Comprehensive cellulose chemistry: fundamentals and analytical methods. Wiley-VCH; 1998.
[53] Hu TQ. Chemical modification, properties, and usage of lignin. New York, NY: Kluwer Academic/Plenum Publishers; 2002.
[54] Cai J, Wu W, Liu R. Sensitivity analysis of three-parallel-DAEM-reaction model for describing rice straw pyrolysis. Bioresour Technol 2013;132:423–6.
[55] Cai JM, Wu WX, Liu RH, Huber GW. A distributed activation energy model for the pyrolysis of lignocellulosic biomass. Green Chem 2013;15:1331–40.
[56] Gašparoviè L, Labovský J, Markoš J, Jelemenský L. Calculation of kinetic parameters of the thermal decomposition of wood by distributed activation energy model (DAEM). Chem Biochem Eng Q 2012;26:45–53.
[57] Ferdous D, Dalai AK, Bej SK, Thring RW. Pyrolysis of lignins: experimental and kinetics studies. Energy Fuels 2002;16:1405–12.
[58] Beis SH, Mukkamala S, Hill N, Joseph J, Baker C, Jensen B, et al. Fast pyrolysis of lignins. Bioresources 2010;5:1408–24.
[59] Janković B. The comparative kinetic analysis of Acetocell and Lignoboost® lignin pyrolysis: the estimation of the distributed reactivity models. Bioresour Technol 2011;102:9763–71.
[60] Wu M, Varhegyi G, Zha Q. Kinetics of cellulose pyrolysis after a pressurized heat treatment. Thermochim Acta 2009;496:59–65.
[61] Please CP, McGuinness MJ, McElwain DLS. Approximations to the distributed activation energy model for the pyrolysis of coal. Combust Flame 2003;133:107–17.
[62] Cai JM, Liu RH. Parametric study of the nonisothermal nth-order distributed activation energy model involved the Weibull distribution for biomass pyrolysis. J Therm Anal Calorim 2007;89:971–5.
[63] Sonoyama N, Hayashi J-I. Characterisation of coal and biomass based on kinetic parameter distributions for pyrolysis. Fuel 2013;114:206–15.
[64] Sonobe T, Worasuwannarak N. Kinetic analyses of biomass pyrolysis using the distributed activation energy model. Fuel 2008;87:414–21.
[65] Li Z, Liu C, Chen Z, Qian J, Zhao W, Zhu Q. Analysis of coals and biomass pyrolysis using the distributed activation energy model. Bioresour Technol 2009;100:948–52.
[66] Li L, Wang G, Wang S, Qin S. Thermogravimetric and kinetic analysis of energy crop Jerusalem artichoke using the distributed activation energy model. J Therm Anal Calorim 2013;114:1183–9.
[67] Soria-Verdugo A, Garcia-Hernando N, Garcia-Gutierrez LM, Ruiz-Rivas U. Analysis of biomass and sewage sludge devolatilization using the distributed activation energy model. Energy Convers Manage 2013;65:239–44.
[68] Várhegyi G, Chen HG, Godoy S. Thermal decomposition of wheat, oat, barley, and brassica carinata straws. A kinetic study. Energy Fuels 2009;23:646–52.
[69] Wang G, Li W, Li BQ, Chen HK. TG study on pyrolysis of biomass and its three components under syngas. Fuel 2008;87:552–8.